



A simple strategy to improve Pd dispersion and enhance Pd/TiO₂ catalytic activity for formaldehyde oxidation: The roles of surface defects

Chunying Wang^{a,d}, Yaobin Li^{a,b,*}, Changbin Zhang^{c,d}, Xueyan Chen^{c,d}, Chunli Liu^e,
Weizheng Weng^e, Wenpo Shan^{a,b}, Hong He^{a,b,c,d,*}

^a Center for Excellence in Regional Atmospheric Environment, Key Laboratory of Urban Pollutant Conversion, Institute of Urban Environment, Chinese Academy of Sciences, Xiamen 361021, China

^b Zhejiang Key Laboratory of Urban Environmental Processes and Pollution Control, Ningbo Urban Environment Observation and Research Station, Chinese Academy of Sciences, Ningbo 315800, China

^c State Key Joint Laboratory of Environment Simulation and Pollution Control, Research Center for Eco-environmental Sciences, Chinese Academy of Sciences, Beijing 100085, China

^d University of Chinese Academy of Sciences, Beijing 100049, China

^e State Key Laboratory of Physical Chemistry of Solid Surfaces, National Engineering Laboratory for Green Chemical Productions of Alcohols, Ethers and Esters, Department of Chemistry, College of Chemistry and Chemical Engineering, Xiamen University, Xiamen 361005, China

ARTICLE INFO

Keywords:

Surface defects
HTR
SMSI
Palladium
Formaldehyde

ABSTRACT

Highly dispersed precious metals are critical to many important catalytic reactions and strongly affect the activity of catalysts. In this work, a simple method to stabilize noble metals on Pd/TiO₂ catalyst by constructing Ti³⁺ defects on the surface of TiO₂ supports. The TiO₂ samples with different contents of Ti³⁺ defects were used to prepare a series of Pd/TiO₂ catalysts, which were tested in formaldehyde (HCHO) oxidation. Multiple characterization results illustrated that the Ti³⁺ defects on TiO₂ produced by hydrogen pretreatment during high temperature reduction (HTR), favored the stabilization of Pd particles through the strong metal-support interaction (SMSI). The increasing Pd dispersion induced more oxygen vacancies on the surfaces of Pd/TiO₂ catalysts, because of hydrogen spillover, and further increased the electron density of Pd species. The activation of water and oxygen was also promoted to form more surface oxygen species. Therefore, the more surface defects existing, the better performance of Pd/TiO₂ catalysts displayed for HCHO oxidation.

1. Introduction

HCHO is one of the main indoor pollutants and is emitted from a wide range of sources, such as building/furnishing materials and decorative products [1,2]. Long-time exposure to HCHO, even at low concentrations, may induce health problems such as nasal tumors, headache, eye irritation, respiratory tract diseases or even cancer [3]. Catalytic oxidation is widely recognized as a promising method for HCHO removal because of its high effectiveness in catalyzing HCHO oxidation, which can convert HCHO into harmless CO₂ and H₂O without any secondary pollution [4,5]. Compared to metal oxide catalysts (Ce, Mn, Co, Ni) where higher reaction temperature is needed [6–13], noble metal (Pt, Au, Pd, Ir, Rh) catalysts are considered to be more suitable for indoor HCHO elimination due to their excellent performance in HCHO oxidation at room temperature [11,14–17]. However, the high cost of noble metal catalysts has limited their wide

application. Therefore, it is necessary to further improve their performance for HCHO oxidation or cut down the application cost.

Surface defects, generally thought to have a profound influence on the chemical properties of metal oxide, play important roles in the burgeoning range of applications involving geochemistry, gas sensors, microelectronics and especially catalytic fields [18]. Especially in the field of heterogeneous catalysis, surface defects were crucial in catalysts or catalytic supports. Some reports recorded that defects of metal oxides, metal sulfides, metal nitrides, and metal-organic frameworks (MOFs) were applied to anchor the single atomic metal sites through surface disorder, dislocation, heterogeneity, and vacancy, due to the SMSI [19–21]. Oxygen vacancy is a dominant type of defects in many metal oxides and had been widely investigated by theoretical calculations and experimental characterization [22–25]. It has been found that oxygen vacancies play important roles as active sites for heterogeneous catalysis, which strongly affect the activity of the catalysts [24]. It is

* Corresponding authors at: Center for Excellence in Regional Atmospheric Environment, Key Laboratory of Urban Pollutant Conversion, Institute of Urban Environment, Chinese Academy of Sciences, Xiamen 361021, China.

E-mail addresses: ybli@iue.ac.cn (Y. Li), honghe@rcees.ac.cn (H. He).

<https://doi.org/10.1016/j.apcatb.2020.119540>

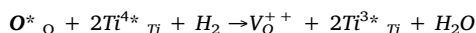
Received 25 May 2020; Received in revised form 28 July 2020; Accepted 4 September 2020

Available online 09 September 2020

0926-3373/ © 2020 Elsevier B.V. All rights reserved.

worth noting that oxygen vacancies on TiO₂ are important active sites for water dissociation to form surface hydroxyl groups [26,27], which are essential for some reactions, such as CO oxidation [28,29], water gas shift (WGS) [30] and HCHO catalytic oxidation [31–36]. For HCHO oxidation, oxygen vacancy involved in many research works was just one of the factors that affected the performance of catalysts, especially in the supported catalysts [31–35,37,38]. Therefore, the investigation about influence of surface defects on the supported catalysts was not comprehensive. The influence mechanism of defects on catalyst structure, especially on the noble metals was still not got attention in HCHO oxidation studies. In our previous work, we found an interesting phenomenon that high temperature reduction did not lead in agglomeration of Pd particles but did promote the Pd dispersion. We attributed the phenomenon to TiO_{2-x}, which diffused to the surface of Pd particles and then embedded them [33]. Based on this discovery, we put forward another interesting assumption that the surface defects of carriers produced by high temperature treatment, may play a key role in trapping the Pd particles, which is worth exploring.

As we know, surface defects can be formed by high-temperature heating under ultra-high vacuum or a reducing atmosphere, high-energy particle bombardment and ion or γ -ray sputtering, etc. [25,39–43]. Among these methods, high-temperature reduction is a simple and effective way to produce surface defects (Ti³⁺ species and oxygen vacancies) on TiO₂ according to the Kröger-Vink equation [25,44]:



(where O^*_{O} is an O²⁻ ion in the oxygen lattice site, V^{+}_{O} is an oxygen vacancy with double positive charge, Ti^{4*}_{Ti} is a Ti⁴⁺ ion in the titanium lattice site, and Ti^{3*}_{Ti} is a Ti³⁺ ion in the titanium lattice site.)

In this study, to obtain different amount of defects on the carriers, TiO₂ was firstly pretreated with H₂ at different temperatures (200, 400 and 600 °C). Then, a series of Pd/TiO₂ catalysts were prepared using the pretreated TiO₂ samples as carriers. It was found that pretreatment at higher temperature contributed to better performance in HCHO oxidation. Complete conversion of 150 ppm HCHO at a WHSV of 300,000 mL/(g h) could be achieved on the Pd/TiO₂-600 catalyst at room temperature. The catalysts were then characterized by CO chemisorption, high-angle annular dark-field scanning transmission electron microscopy (HAADF-STEM), temperature programmed reduction by H₂ (H₂-TPR), electron spin resonance (ESR), temperature-programmed desorption by CO₂ (CO₂-TPD), Fourier transform infrared (FTIR), X-ray photoelectron spectroscopy (XPS) and in situ Diffuse Reflectance Infrared Fourier Transform Spectroscopy (in situ DRIFTS). Based on the characterization results, the effects of surface defects were discussed and elucidated.

2. Experiment section

2.1. Catalyst preparation

A series of 1 wt. % Pd/TiO₂ catalysts were prepared by impregnation of TiO₂ (Alfa Aesar) with aqueous Pd(NO₃)₂ (Sigma Aldrich), according to our previous study [15]. In this study, however, TiO₂ was pretreated with a gas mixture of 10 vol. % H₂/N₂ at different temperatures (200, 400 and 600 °C) and marked as TiO₂-200, TiO₂-400 and TiO₂-600, respectively. Before activity testing and characterization, the samples were reduced with H₂ at 350 °C for 1 h. After that the catalysts were labeled as Pd/TiO₂, Pd/TiO₂-200, Pd/TiO₂-400 and Pd/TiO₂-600, respectively.

2.2. Catalyst characterization

X-ray diffraction (XRD), N₂ adsorption-desorption, CO pulse chemisorption, H₂-TPR, XPS, HAADF-STEM analysis and FTIR spectra were carried out according to our previous work [33]. In situ DRIFT spectra

were recorded on a Thermo Fisher IS50 FTIR spectrometer, equipped with an in situ diffuse reflectance chamber (Harrick) and high sensitivity MCT/A detector. Before recording each DRIFT spectrum, the sample was reduced in situ in H₂ flow at 623 K for 1 h, then purged with He flow for 30 min, followed by cooling down to 25 °C. All spectra were measured with a resolution of 4 cm⁻¹ and an accumulation of 100 scans.

ESR spectra were collected on a Benchtop Micro-ESRTM machine (Active Spectrum, Inc.). The ESR spectra were performed at a microwave frequency of 9.70 GHz at 120 K without light irradiation. The scanning speed was 30 s per sweep, and the spectra were averaged based on 30 sweeps. The UV–vis absorption spectra were measured by a Shimadzu UV-3600 UV–vis spectrophotometer.

CO₂-TPD was performed on a Micromeritics AutoChem II 2920 apparatus. Firstly, the catalysts were reduced in situ with 10 vol. % H₂/Ar flow at 623 K for 1 h, then cooled down to 80 °C by purging with Ar. After that the system was switched to 5 vol. % O₂/He for 1 h, then purged with Ar for 40 min, followed by cooling down to -10 °C. Then the system was switched to 5 vol. % CO/He for 30 min, followed by purging with Ar for another 20 min. Finally, CO₂-TPD was conducted in He from -10 to 800 °C at a rate of 10 °C/min. The product (CO₂) was monitored using a mass spectrometer.

2.3. Activity test for HCHO oxidation

The activity tests for the catalytic oxidation of HCHO on the catalysts (20 mg) were performed in a fixed-bed quartz flow reactor (d = 4 mm) in an incubator kept at 25 °C. Gaseous HCHO was generated by flowing He through a para-formaldehyde container. Water vapor was generated by flowing He through a water bubbler. The feed gas composition was 150 ppm of HCHO, 20 % O₂, 35 % RH and He balance. The total flow rate was 100 mL/min, corresponding to a WHSV of 300,000 mL/(g h). The inlet and outlet gases were monitored according to our previous work [32]. In all the experiments, HCHO conversion was calculated using the following equation:

$$HCHO\ Conversion(\%) = \left(1 - \frac{[HCHO]_{out}}{[HCHO]_{in}} \right) \times 100\%$$

The CO₂ yield was defined as follows:

$$CO_2\ Yield(\%) = \frac{[CO_2]}{[HCHO]_{in}} \times 100\%$$

where [HCHO]_{in} and [HCHO]_{out} are the inlet and outlet HCHO concentrations, [CO₂] is the outlet CO₂ concentration, respectively.

Turnover frequency (TOF, s⁻¹) was calculated at 25 °C based on a separate experiment where the apparent conversion of HCHO was kept below 20 % by varying the inlet HCHO concentration and WHSV, with negligible heat and mass-transfer effects and TOF was calculated according to the following equation [33]:

$$TOF = \frac{n_{HCHO}}{n_{Pd}} = \frac{[HCHO]_{in} \times \gamma \times V/R_g}{m_{cat} \times \omega_{Pd} \times D_{Pd}/M_{Pd}}$$

Where the parameters are the molar weight of consumed HCHO per second (n'_{HCHO} , mol s⁻¹), molar weight of Pd exposed on TiO₂ surface (n'_{Pd} , mol), initial inlet concentration of HCHO ([HCHO]_{in}, ppm), total flow rate (V, L s⁻¹), molar volume of gas at 25 °C and 101 kPa (R_g , 24.5 L mol⁻¹), weight of catalyst (m_{cat} , g), loading percentage of Pd (ω_{Pd} , %), Pd dispersion (D_{Pd} , %) and molecular mass of Pd (M_{Pd} , g mol⁻¹), respectively.

3. Results and discussion

3.1. Structure of catalysts

The specific surface areas were determined by N₂ adsorption-

Table 1

Specific Surface Area (S_{BET}), Pd Dispersion (d), difference value between d_{TEM} and d_{CO} , Pd nanoparticles size (D) and turnover frequencies (TOF) of Pd/TiO₂, Pd/TiO₂-200, Pd/TiO₂-400 and Pd/TiO₂-600 catalysts.

Samples	S_{BET} (m ² /g)	d_{CO}^{a} (%)	$d_{\text{TEM}}^{\text{b}}$ (%)	$d_{\text{TEM}}-d_{\text{CO}}$ (%)	$D_{\text{TEM}}^{\text{c}}$ (nm)	TOF $\times 10^{-3}$ ^d (s ⁻¹)
Pd/TiO ₂	59.7	13.9	20.8	6.9	3.32	3.59
Pd/TiO ₂ -200	57.4	14.3	22.7	8.4	3.04	7.06
Pd/TiO ₂ -400	57.8	18.0	31.8	13.8	2.17	10.31
Pd/TiO ₂ -600	50.6	21.3	39.6	18.3	1.74	30.84

^a Pd dispersion measured with CO pulse chemisorption.

^b Pd dispersion calculated based on D_{TEM} .

^c Pd particle size measured with TEM.

^d Turnover frequencies (TOF) calculated from d_{TEM} .

desorption analysis and the results are exhibited in Table 1. After pretreatment at high temperature, the surface area slightly decreased from 59.7 m²/g to 50.6 m²/g due to TiO₂ pores collapsing during reduction. The XRD patterns of reduced Pd/TiO₂ catalysts and TiO₂ supports are shown in Fig. S1. The results displayed there was no change in the crystal structures of all the carriers and catalysts, indicating that the reduction temperature had little influence on their crystal structures and that Pd was well dispersed.

3.2. Defects analysis

In order to measure the defects on the pretreated TiO₂ carriers, ESR and diffuse reflectance UV-vis-NIR spectra were measured and the results are displayed in Fig. 1. The ESR signals of the TiO₂ supports are displayed in Fig. 1a. All of the samples showed a signal at $g = 1.977$, which is ascribed to Ti³⁺ [45]. Notably, the signal of Ti³⁺ became stronger in the order of TiO₂, TiO₂-200, TiO₂-400 and TiO₂-600, which implied that reduction treatment could induce surface defects on the TiO₂ nanocrystals, that is, the higher reduction temperature, the more surface defects. As shown in Fig. 1b, the results of diffuse reflectance UV-vis-NIR spectroscopy further verified the above conclusions. After treatment with H₂ at 200, 400, and 600 °C, TiO₂ samples exhibited an absorption located in the visible and NIR region, which was due to the transitions of electrons in shallow traps or the conduction band [46]. The absorption intensity gradually increased as the treatment temperature rose, which indicated that defects were enhanced with increasing reduction temperature. After Pd loading (Fig. 2a), besides Ti³⁺ species, a new species at $g = 2.004$ appeared on the four Pd/TiO₂ catalysts, which is assigned to oxygen vacancies [47]. In addition, the amount of oxygen vacancies was increasing in the order of Pd/TiO₂ < Pd/TiO₂-200 < Pd/TiO₂-400 < Pd/TiO₂-600 catalyst, which was in line with the result of diffuse reflectance UV-vis-NIR spectroscopy of the four catalysts. As shown in Fig. 2b, the photo-absorption edges caused by interband transition occurred at approximately 410 nm

on the four catalysts, which is characteristic of doped TiO₂ with mid-gap impurity states. The absorption intensity gradually increased in the order of Pd/TiO₂ < Pd/TiO₂-200 < Pd/TiO₂-400 < Pd/TiO₂-600 catalysts, implied the doping degree of catalyst is improved. Compared to the diffuse reflectance UV-vis-NIR spectroscopy of supports, the photo-absorption intensities were all enhanced, which indicated that after loading Pd species there were more defects formed. The reason why the amount of oxygen vacancies increasing with the carriers pretreatment temperature rising will be further elucidated.

3.3. Pd dispersion and particle size analysis

CO pulse chemisorption was carried out to determine the Pd dispersion (d_{CO}) and the results are listed in Table 1. Pd dispersion on the Pd/TiO₂, Pd/TiO₂-200, Pd/TiO₂-400 and Pd/TiO₂-600 catalysts was 13.9 %, 14.3 %, 18.0 %, and 21.3 %, respectively. To verify the above phenomenon, Pd particle size distributions were further measured using HAADF/STEM, and the results are shown in Fig. 3 and Table 1. The mean Pd particle size was 3.32, 3.04, 2.17 and 1.74 nm on Pd/TiO₂, Pd/TiO₂-200, Pd/TiO₂-400 and Pd/TiO₂-600 catalysts, respectively, which was in accordance with the Pd dispersion results. The elemental mapping diagram displayed the spatial distribution of TiO₂ and Pd nanoparticles, which implied that Pd distributed uniformly and further confirmed the dispersion of Pd particles on the four catalysts gradually increased (shown in Fig. S2). The above results implied that HTR treatment of the carriers was beneficial to Pd dispersion even in the case of a decrease in surface specific area. It was reported that surface defects on carriers, such as metal sulfides, metal oxides and metal-organic frameworks, play an important role in anchoring the supported metal ions to prepare single-atom catalysts [19,21,48,49]. The DFT calculations also confirmed that the interaction between the Pd atom and the oxygen-vacant TiO₂(101) surface is remarkably stronger than that between the Pd atom and the intrinsic TiO₂(101) surface with respect to the adsorption energy [50]. Combining with the result of Fig. 1, it is reasonable to attribute the enhancement of Pd dispersion to the more surface defects formed on TiO₂. It is noteworthy that better Pd dispersion means more active sites for hydrogen spillover in the process of reduction. Therefore, the phenomenon that the amount of oxygen vacancies increasing in the order of Pd/TiO₂ < Pd/TiO₂-200 < Pd/TiO₂-400 < Pd/TiO₂-600 catalyst (observed in Fig. 2) could be attributed to the enhanced Pd dispersion. Meanwhile, a SMSI between Pd particles and TiO₂ was also formed.

The Pd dispersion based on D_{TEM} was also calculated and labeled as d_{TEM} and the value is shown in Table 1. Theoretically, the value of d_{CO} approaches that of d_{TEM} . According to a previous work [14], the existence of a SMSI could induce suppression of the adsorption of small molecules such as CO and H₂ [51–53]. In this work, for all the Pd/TiO₂ catalysts, the values of d_{CO} were smaller than d_{TEM} , which confirmed the existence of a SMSI on the Pd/TiO₂ catalysts. Meanwhile, as the TiO₂

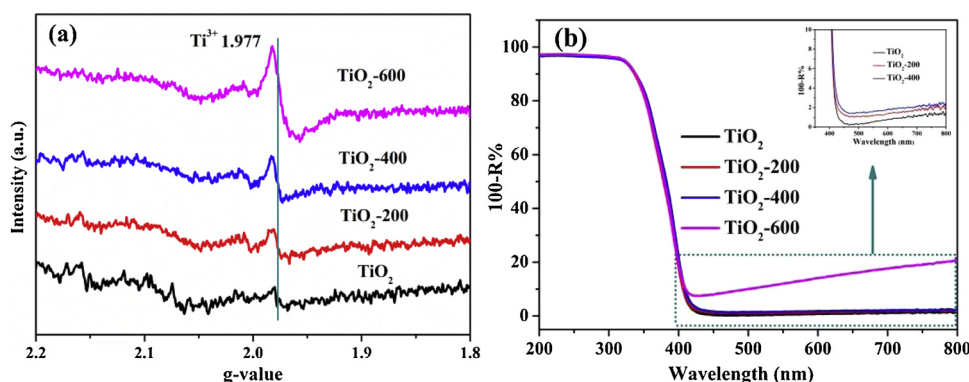


Fig. 1. ESR (a) and diffuse reflectance UV-vis-NIR spectra (b) of TiO₂, TiO₂-200, TiO₂-400 and TiO₂-600 carriers.

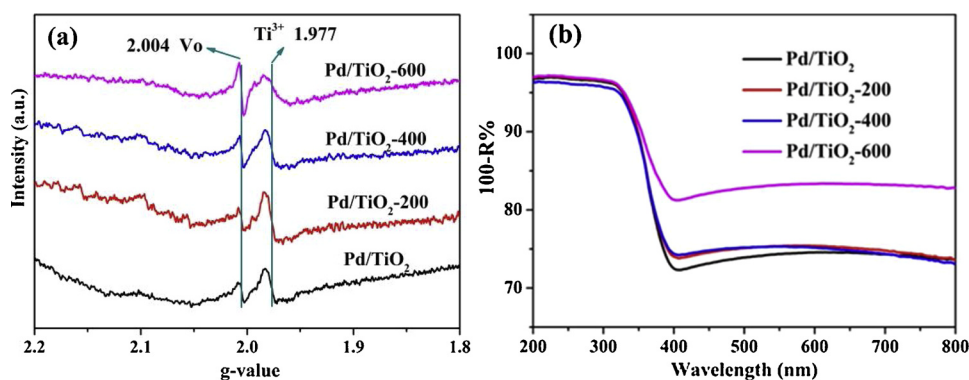


Fig. 2. ESR (a) and diffuse reflectance UV-vis-NIR spectra (b) of Pd/TiO₂, Pd/TiO₂-200, Pd/TiO₂-400 and Pd/TiO₂-600 samples.

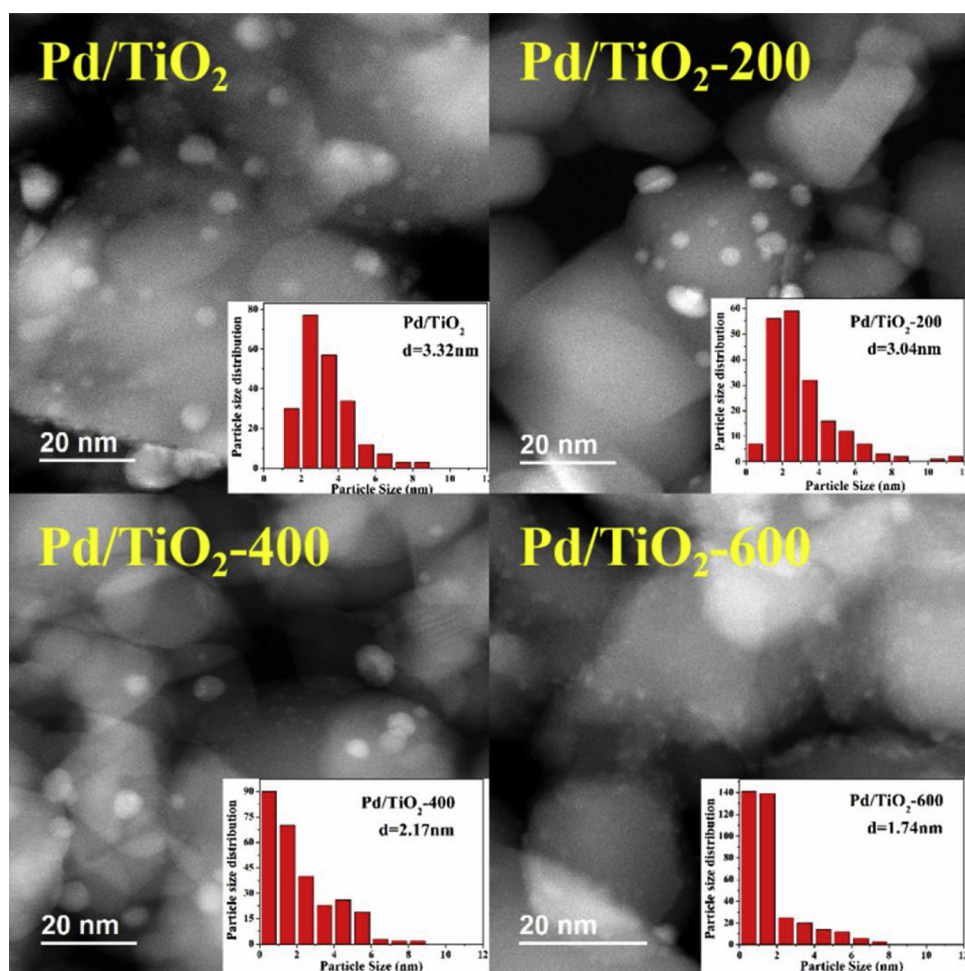


Fig. 3. HAADF/STEM images and particle size distribution of Pd/TiO₂, Pd/TiO₂-200, Pd/TiO₂-400 and Pd/TiO₂-600 samples.

reduction temperature increase, the difference between d_{TEM} and d_{CO} grew larger; that is, the strength of the SMSI was enhanced. The phenomenon was also seen on the HRTEM pictures (shown in Fig. S3), and some encapsulated Pd nanoparticles were observed (marked by red circles). Obviously, with the increase of pretreatment temperature of catalysts, the number of coated particles increased gradually, which indicated the SMSI between Pd and TiO₂ was become stronger.

3.4. XPS analysis

To demonstrate the electronic states of Pd and O elements on the catalyst surface, XPS measurements of Pd 3d and O 1s were carried out

next and the results are shown in Fig. 4. As shown in Fig. 4a, three kinds of Pd species were observed on all of the Pd/TiO₂-X catalysts. The peak in the range of 336.4–336.7 eV was assigned to Pd²⁺ species, which may be attributed to the re-oxidation of metal Pd particles by O₂ and/or H₂O in air during transfer of the sample to the XPS chamber [45]. The peaks in the range of 334.1–335.4 eV should be attributed to Pd⁰ species. Different from the Pd species at 335.0–335.4 eV, the ones at 334.1–334.4 eV possessed more electrons, and should be ascribed to Pd^{δ-} species interacting with oxygen vacancies, represented by Pd^{δ-}}-Vo. The negatively charged Pd^{δ-} species resulted from electron transfer from the oxygen vacancies to Pd^{δ-} groups through the SMSI between Pd particles and TiO₂ [15,54] and the DFT result proved that the Hirshfeld charge of

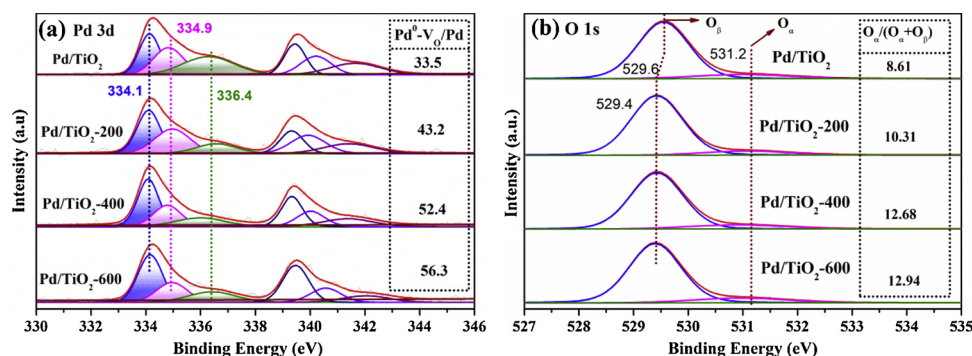


Fig. 4. XPS spectra of Pd/TiO₂, Pd/TiO₂-200, Pd/TiO₂-400 and Pd/TiO₂-600 samples, (a) Pd 3d (inset: Distribution ratio of Pd^δ-V_o/Pd); (b) O 1s (inset: Distribution ratio of O_α/(O_α+O_β)).

Pd atom was lower and closer to the metallic state over TiO_{2-x} support with oxygen vacancies than that over intrinsic TiO₂ support [55]. It was reported that negatively charged noble metal nanoparticles could enhance O₂ adsorption and activation, because the electron donation from the metal to the antibonding π^* orbital of O₂ was enhanced [38]. The relative contents of Pd^δ-V_o species were calculated, and they were 33.5%, 43.2%, 52.4% and 56.3% on Pd/TiO₂, Pd/TiO₂-200, Pd/TiO₂-400 and Pd/TiO₂-600, respectively. As can be seen, higher reduction temperature was associated with the production of more Pd^δ-V_o species, in line with the HCHO oxidation activity.

Fig. 4b displays the O 1s XPS spectra of the catalysts. All samples exhibited peaks of two kinds of O species. The main peak in the range of 529.4–529.6 eV was ascribed to the lattice oxygen of bulk TiO₂ (O_β) [56]. The shoulder peak in the range of 531.2–531.4 eV may be assigned to chemisorbed oxygen (O_α) [32,57]. The ratio of O_α/(O_α+O_β) slightly increased with the increase of the carrier pretreatment temperature, and Pd/TiO₂-600 possessed the most chemisorbed oxygen species. The results indicated the presence of a large amount of surface oxygen species on Pd/TiO₂-600 catalyst, consistent with its excellent ability to activate water and oxygen. The result was also confirmed by CO₂-TPD (as shown in Fig. 5). Clearly, the peak area of desorbed CO₂ gradually increased in the order of Pd/TiO₂, Pd/TiO₂-200, Pd/TiO₂-400 and Pd/TiO₂-600. The phenomenon indicated that active oxygen was indeed enhanced on the catalysts after the carriers were pretreated by HTR and that this active oxygen could oxidize CO to CO₂ [58].

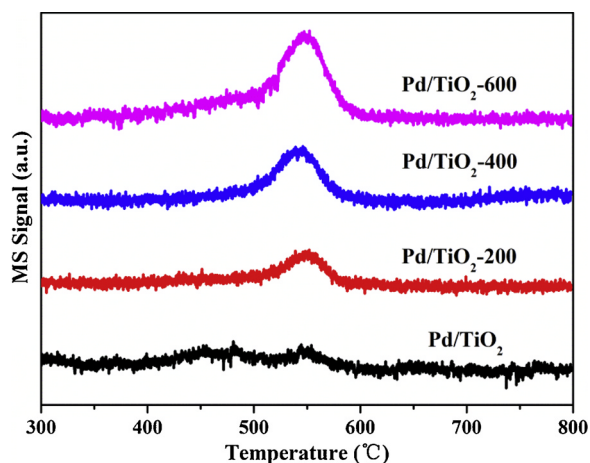


Fig. 5. CO₂-TPD of Pd/TiO₂, Pd/TiO₂-200, Pd/TiO₂-400 and Pd/TiO₂-600 samples. Reaction conditions: the catalysts were reduced in situ with H₂/Ar flow at 623 K for 1 h, then the catalyst preabsorbs O₂/He for 1 h, followed by purging with Ar and cooling down to -10 °C. After that, the catalyst preabsorbs 5 vol. % CO/He for 30 min. Finally, the system programmed temperature desorption and CO₂ was tested by MS detector.

3.5. Water activation capacity test

It is worth noting that oxygen vacancies are important active sites for water dissociation to form surface hydroxyl groups [42]. FTIR measurements were carried out to further investigate the surface hydroxyl groups, and the results are shown in Fig. 6. All four samples displayed two peaks at 1629 cm⁻¹ and 3424 cm⁻¹, which are assigned to the bending and stretching vibrations of surface OH, respectively [59,60]. It was apparent that the amount of surface OH species followed the order Pd/TiO₂ < Pd/TiO₂-200 < Pd/TiO₂-400 < Pd/TiO₂-600, which was in line with the O 1s XPS results. This result indicated that treatment of the carrier with HTR could enhance the ability of Pd/TiO₂ catalysts to activate water molecules to form surface OH groups. As mentioned above, with increasing TiO₂ pretreatment temperature, more oxygen vacancies appeared on the Pd/TiO₂ catalysts. As is well known, oxygen vacancies play an important role in water dissociation to form surface active OH groups [14,61–63].

3.6. Reducibility of catalysts

The effect of pretreatment of the supports on the reducibility of the catalysts was investigated by H₂-TPR measurements, and the results are shown in Fig. 7. The catalysts exhibited two peaks in the temperature range of -50–100 °C. The negative peak at around 75 °C is associated with hydrogen desorption from PdH₄ [64]. The main hydrogen consumption peaks of the Pd/TiO₂, Pd/TiO₂-200, Pd/TiO₂-400 and Pd/TiO₂-600 catalysts were below zero °C at -6.9, -8.4, -9.0 and -10.4 °C

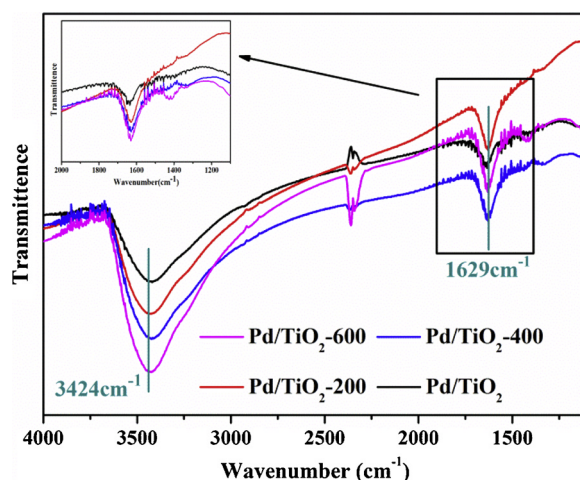


Fig. 6. The hydroxyl groups test by FTIR of Pd/TiO₂, Pd/TiO₂-200, Pd/TiO₂-400 and Pd/TiO₂-600 samples. Reaction condition: 1 mg samples was mixed with 150 mg KBr followed drying under a heat lamp, then the mixture was pressed into a transparent pellet die before FTIR tests.

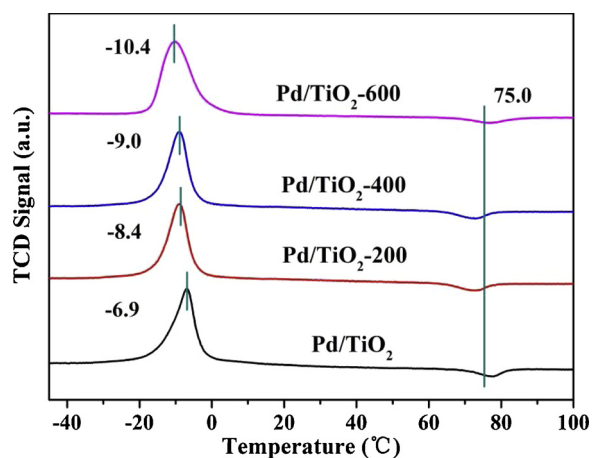


Fig. 7. H₂-TPR of the unreduced Pd/TiO₂, Pd/TiO₂-200, Pd/TiO₂-400 and Pd/TiO₂-600 catalysts.

respectively, which were assigned to the reduction of Pd²⁺ species [65]. With increasing pretreatment temperature for the supports, the hydrogen consumption peaks gradually shifted to lower temperatures, which suggested that the reducibility of catalysts was enhanced.

3.7. Activity in HCHO oxidation

The performance of Pd/TiO₂, Pd/TiO₂-200, Pd/TiO₂-400 and Pd/TiO₂-600 in HCHO oxidation was evaluated and the results are shown in Fig. 8. For the catalysts, HCHO conversion was 2%, 15%, 23% and 100% at 25 °C, respectively. With reaction temperature increasing, the HCHO conversion ratio of Pd/TiO₂, Pd/TiO₂-200, Pd/TiO₂-400 catalysts increased and reached 80%, 96% and 100% at 135 °C, respectively. Meanwhile, from Fig. S4, there were no other by-products besides CO₂. It was clear that the catalytic activity of HCHO oxidation improved with increasing carrier pretreatment temperature. Moreover, as shown in Fig. S5, the Pd/TiO₂-600 catalyst displayed an excellent stability, maintaining 100% conversion at a high WHSV (300,000 mL/g h for 20 h).

Based on the results of Pd dispersion (d_{co}), TOFs over the four catalysts were calculated at 25 °C and the results are summarized in Table 1. The Pd/TiO₂, Pd/TiO₂-200, Pd/TiO₂-400 and Pd/TiO₂-600 catalysts presented TOFs of 3.59×10^{-3} , 7.06×10^{-3} , 10.31×10^{-3} and $30.84 \times 10^{-3} \text{ s}^{-1}$, respectively. It is clear that the HTR treatment of the supports significantly enhanced the intrinsic catalytic activity of the Pd/TiO₂ catalysts.

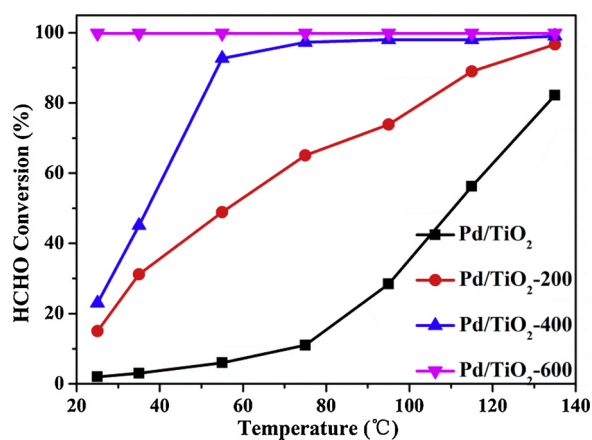


Fig. 8. HCHO conversion over Pd/TiO₂, Pd/TiO₂-200, Pd/TiO₂-400 and Pd/TiO₂-600 samples. Reaction conditions: 150 ppm of HCHO, 20% O₂, 35% RH, He balance, WHSV 300,000 mL/(g·h).

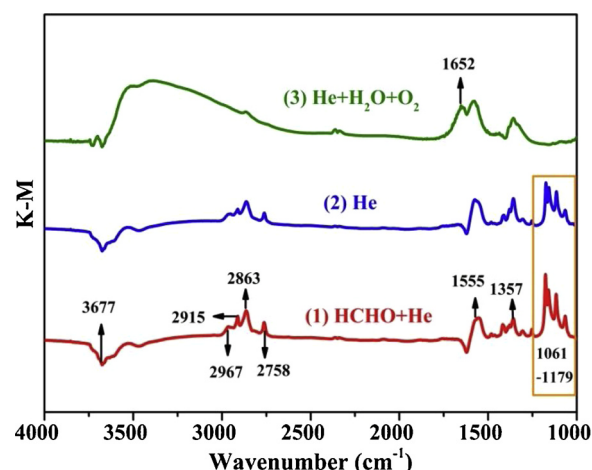


Fig. 9. In situ DRIFTS spectra over Pd/TiO₂-600 in a flow of HCHO for 60 min (1); followed by He purging for 60 min (2); and by O₂ + H₂O + He purging for 60 min (3) at room temperature. Reaction conditions: 230 ppm of HCHO, 20% O₂, 35% RH, He balance, total flow rate of 100 mL/min.

3.8. Reaction pathways of HCHO oxidation

The reaction mechanisms of HCHO oxidation on the Pd/TiO₂ catalysts at room temperature were investigated with in situ DRIFTS. The spectra of the Pd/TiO₂-600 catalyst at steady state under different gas flows are shown in Fig. 9. Firstly, the Pd/TiO₂-600 catalyst was exposed to a flow of HCHO + He for 60 min. With the consumption of surface hydroxyl species (3677 cm^{-1} for $\nu(\text{OH})$) [14], other species, including dioxyethylene (DOM) species ($1061 - 1179 \text{ cm}^{-1}$) and formate species ($1357, 1555 \text{ cm}^{-1}$ for $\nu(\text{COO})$ and $2758, 2863$ and 2915 cm^{-1} for $\nu(\text{C-H})$), appeared due to partial oxidation of adsorbed HCHO by residual surface OH groups [10,14,33,66–69]. After HCHO adsorption saturation, the system was purged by He for 60 min. The bands of DOM species decreased slightly, meanwhile the bands of formate species increased, which was due to the decomposition of DOM by the active hydroxyl groups. However, there were not enough oxygen species to entirely oxidize the DOM species. When water and oxygen were introduced into the system, the DOM species almost entirely disappeared, while the formate groups did not significantly increase and the CO₂ species (2350 cm^{-1}) simultaneously appeared. The phenomenon further implied that surface active oxygen groups played an important role not only in DOM conversion but also in the formate decomposition process. Based on the results shown in Fig. S6, HCHO oxidation on the Pd/TiO₂ catalysts followed the same reaction pathway, and formate oxidation was the rate-controlling step. Thus, the pre-reduction of the carriers may have no impact on the HCHO oxidation pathway on the Pd/TiO₂ catalysts.

4. Conclusions

A series of Pd/TiO₂ catalysts were prepared with different amounts of Ti³⁺ defects on carriers treated by HTR. It is clear that TiO₂ surface defects formed by HTR played important roles in HCHO oxidation. On the one hand, Pd ions could be trapped by surface defects and Pd dispersion will be improved. The catalysts with a better Pd dispersion possess more active sites for HCHO oxidation and hydrogen spillover. So there were more oxygen vacancies formed on the catalysts surfaces. Meanwhile, the presence of more Pd-Vo species increased the electron density around Pd species and enhanced the activation of chemisorbed oxygen, which is beneficial to HCHO catalytic oxidation. On the other hand, as we know, the more oxygen vacancies exist on the catalysts, the more OH groups can be produced. Therefore, with increasing pre-reduction temperature of TiO₂, the performance of Pd/TiO₂ catalysts for

HCHO oxidation improved. The Pd/TiO₂-600 catalyst could completely convert HCHO into CO₂ and H₂O at 25 °C with a WHSV of 300,000 mL/(g h).

CRedit authorship contribution statement

Chunying Wang: Writing - original draft, Validation, Software.
Yaobin Li: Conceptualization, Investigation, Writing - review & editing, Supervision, Funding acquisition.
Changbin Zhang: Writing - review & editing, Visualization.
Xueyan Chen: Software, Visualization.
Chunli Liu: Data curation.
Weizheng He: Data curation.
Wenpo Shan: Writing - review & editing.
Hong He: Conceptualization, Supervision, Writing - review & editing.

Declaration of Competing Interest

The authors declare that they have no known competing financial interests or personal relationships that could have appeared to influence the work reported in this paper.

Acknowledgements

This work was financially supported by the National Natural Science Foundation of China (21707136) and Natural Science Foundation of Fujian Province, China (2018J05027)

Appendix A. Supplementary data

Supplementary material related to this article can be found, in the online version, at doi:<https://doi.org/10.1016/j.apcatb.2020.119540>.

References

- E. Hult, H. Willem, P. Price, T. Hotchi, M. Russell, B. Singer, Formaldehyde and acetaldehyde exposure mitigation in US residences: In-home measurements of ventilation control and source control, *Indoor Air* 25 (2015) 523–535.
- W. Liang, X. Yang, Indoor formaldehyde in real buildings: emission source identification, overall emission rate estimation, concentration increase and decay patterns, *Build. Environ.* 69 (2013) 114–120.
- X. Sun, J. Lin, H. Guan, L. Li, L. Sun, Y. Wang, S. Miao, Y. Su, X. Wang, Complete oxidation of formaldehyde over TiO₂ supported subnanometer Rh catalyst at ambient temperature, *Appl. Catal. B: Environ.* 226 (2018) 575–584.
- J. Torres, S. Royer, J. Bellat, J. Giraudon, J. Lamonnier, Formaldehyde: Catalytic oxidation as a promising soft way of elimination, *ChemSusChem* 6 (2013) 578–592.
- Y. Chen, J. Gao, Z. Huang, M. Zhou, J. Chen, C. Li, Z. Ma, J. Chen, X. Tang, Sodium rivals silver as single-atom active centers for catalyzing abatement of formaldehyde, *Environ. Sci. Technol.* 51 (2017) 7084–7090.
- M. Wang, L. Zhang, W. Huang, T. Xiu, C. Zhuang, J. Shi, The catalytic oxidation removal of low-concentration HCHO at high space velocity by partially crystallized mesoporous MnOx, *Chem. Eng. J.* 320 (2017) 667–676.
- F. Liu, S. Rong, P. Zhang, L. Gao, One-step synthesis of nanocarbon-decorated MnO₂ with superior activity for indoor formaldehyde removal at room temperature, *Appl. Catal. B: Environ.* 235 (2018) 158–167.
- L. Zhu, J. Wang, S. Rong, H. Wang, P. Zhang, Cerium modified birnessite-type MnO₂ for gaseous formaldehyde oxidation at low temperature, *Appl. Catal. B: Environ.* 211 (2017) 212–221.
- Z. Fan, J. Shi, Z. Zhang, M. Chen, W. Shangguan, Promotion effect of potassium carbonate on catalytic activity of Co₃O₄ for formaldehyde removal, *J. Chem. Technol. Biotechnol.* 93 (2018) 3562–3568.
- H. Wang, W. Guo, Z. Jiang, R. Yang, Z. Jiang, Y. Pan, W. Shangguan, New insight into the enhanced activity of ordered mesoporous nickel oxide in formaldehyde catalytic oxidation reactions, *J. Catal.* 361 (2018) 370–383.
- C. Ma, D. Wang, W. Xue, B. Dou, H. Wang, Z. Hao, Investigation of formaldehyde oxidation over Co₃O₄-CeO₂ and Au/Co₃O₄-CeO₂ catalysts at room temperature: effective removal and determination of reaction mechanism, *Environ. Sci. Technol.* 45 (2011) 3628–3634.
- J. Wang, P. Zhang, J. Li, C. Jiang, R. Yunus, J. Kim, Room-temperature oxidation of formaldehyde by layered manganese oxide: effect of water, *Environ. Sci. Technol.* 49 (2015) 12372–12379.
- S. Lu, K. Li, F. Huang, C. Chen, B. Sun, Efficient MnO_x-Co₃O₄-CeO₂ catalysts for formaldehyde elimination, *Appl. Surf. Sci.* 400 (2017) 277–282.
- Y. Li, X. Chen, C. Wang, C. Zhang, H. He, Sodium enhances Ir/TiO₂ activity for catalytic oxidation of formaldehyde at ambient temperature, *ACS Catal.* 8 (2018) 11377–11385.
- Y. Li, C. Zhang, H. He, J. Zhang, M. Chen, Influence of alkali metals on Pd/TiO₂ catalysts for catalytic oxidation of formaldehyde at room temperature, *Catal. Sci. Technol.* 6 (2016) 2289–2295.
- Q. Xu, W. Lei, X. Li, X. Qi, J. Yu, G. Liu, J. Wang, P. Zhang, Efficient removal of formaldehyde by nanosized gold on well-defined CeO₂ nanorods at room temperature, *Environ. Sci. Technol.* 48 (2014) 9702–9708.
- L. Zhang, L. Chen, Y. Li, Y. Peng, F. Chen, L. Wang, C. Zhang, X. Meng, H. He, F. Xiao, Complete oxidation of formaldehyde at room temperature over an Al-rich Beta zeolite supported platinum catalyst, *Appl. Catal. B: Environ.* 219 (2017) 200–208.
- J. Jupille, G. Thornton, *Defects at Oxide Surfaces*, Springer, 2015.
- J. Liu, Y. Wang, J. Li, Toward rational design of oxide-supported single-atom catalysts: atomic dispersion of gold on ceria, *J. Am. Chem. Soc.* 139 (2017) 6190–6199.
- J. Guzman, S. Carrettin, A. Corma, Spectroscopic evidence for the supply of reactive oxygen during CO oxidation catalyzed by gold supported on nanocrystalline CeO₂, *J. Am. Chem. Soc.* 127 (2005) 3286–3287.
- J. Xie, H. Qu, J. Xin, X. Zhang, G. Cui, X. Zhang, J. Bao, B. Tang, Y. Xie, Defect-rich MoS₂ nanowall catalyst for efficient hydrogen evolution reaction, *Nano Res.* 10 (2017) 1178–1188.
- G. Pacchioni, Oxygen vacancy: the invisible agent on oxide surfaces, *ChemPhysChem* 4 (2003) 1041–1047.
- I. Nakamura, N. Negishi, S. Kutsuna, T. Ihara, S. Sugihara, K. Takeuchi, Role of oxygen vacancy in the plasma-treated TiO₂ photocatalyst with visible light activity for NO removal, *J. Mol. Catal. A Chem.* 161 (2000) 205–212.
- S. Polarz, J. Strunk, V. Ischenko, V. Berg, W. Maurits, O. Hinrichsen, M. Muhler, M. Driess, On the role of oxygen defects in the catalytic performance of zinc oxide, *Angew. Chemie Int. Ed. English* 45 (2006) 2965–2969.
- M. Yang, X. Pan, X. Fu, N. Zhang, Y. Xu, Defective TiO₂ with oxygen vacancies: Synthesis, properties and photocatalytic applications, *Nanoscale* (2013).
- I. Brookes, C. Murny, G. Imaging water dissociation on TiO₂ (110), *Phys. Rev. Lett.* 87 (2001) 266103.
- R. Schaub, P. Thstrup, N. Lopez, E. Lægsgaard, I. Stensgaard, J. Nørskov, F. Besenbacher, Oxygen vacancies as active sites for water dissociation on rutile TiO₂ (110), *Phys. Rev. Lett.* 87 (2001) 266104.
- L. Liu, B. McAllister, H. Ye, P. Hu, Identifying an O₂ supply pathway in CO oxidation on Au/TiO₂ (110): a density functional theory study on the intrinsic role of water, *J. Am. Chem. Soc.* 128 (2006) 4017–4022.
- B. Mukri, G. Dutta, U. Waghmare, M. Hegde, Activation of lattice oxygen of TiO₂ by Pd²⁺ ion: correlation of low-temperature CO and hydrocarbon oxidation with structure of Ti_{1-x}Pd_xO_{2-x} (x = 0.01–0.03), *Chem. Mater.* 24 (2012) 4491–4502.
- G. Jacobs, P. Patterson, U. Graham, A. Crawford, B. Davis, Low temperature water gas shift: the link between the catalysis of WGS and formic acid decomposition over Pt/ceria, *Int. J. Hydrogen Energy* 30 (2005) 1265–1276.
- C. Zhang, F. Liu, Y. Zhai, H. Ariga, N. Yi, Y. Liu, K. Asakura, M. Flytzani-Stephanopoulos, H. He, Alkali-metal-promoted Pt/TiO₂ opens a more efficient pathway to formaldehyde oxidation at ambient temperatures, *Angew. Chem. Int. Ed.* 51 (2012) 9628–9632.
- C. Zhang, Y. Li, Y. Wang, H. He, Sodium-promoted Pd/TiO₂ for catalytic oxidation of formaldehyde at ambient temperature, *Environ. Sci. Technol.* 48 (2014) 5816–5822.
- Y. Li, C. Zhang, J. Ma, M. Chen, H. Deng, H. He, High temperature reduction dramatically promotes Pd/TiO₂ catalyst for ambient formaldehyde oxidation, *Appl. Catal. B: Environ.* 217 (2017) 560–569.
- B. Chen, X. Zhu, M. Crocker, Y. Wang, C. Shi, FeO_x-supported gold catalysts for catalytic removal of formaldehyde at room temperature, *Appl. Catal. B: Environ.* 154–155 (2014) 73–81.
- H. Huang, D. Leung, Complete elimination of indoor formaldehyde over supported Pt catalysts with extremely low Pt content at ambient temperature, *J. Catal.* 280 (2011) 60–67.
- H. Huang, X. Ye, H. Huang, L. Zhang, D. Leung, Mechanistic study on formaldehyde removal over Pd/TiO₂ catalysts: oxygen transfer and role of water vapor, *Chem. Eng. J.* 230 (2013) 73–79.
- M. He, J. Ji, B. Liu, H. Huang, Reduced TiO₂ with tunable oxygen vacancies for catalytic oxidation of formaldehyde at room temperature, *Appl. Surf. Sci.* 473 (2019) 934–942.
- H. Huang, D. Leung, Complete oxidation of formaldehyde at room temperature using TiO₂ supported metallic Pd nanoparticles, *ACS Catal.* 1 (2011) 348–354.
- J. Pan, B. Maschhoff, U. Diebold, T. Madey, Interaction of water, oxygen, and hydrogen with TiO₂ (110) surfaces having different defect densities, *J. Vac. Sci. Technol. A* 10 (1992) 7.
- L. Wang, D. Baer, M. Engelhard, A. Shultz, The adsorption of liquid and vapor water on TiO₂ (110) surfaces: the role of defects, *Surf. Sci.* 344 (1995) 237–250.
- P. Dutta, A. Ginwalla, B. Hogg, B. Patton, B. Chwieroth, Z. Liang, P. Gouma, M. Mills, S. Akbar, Interaction of carbon monoxide with anatase surfaces at high temperatures: optimization of a carbon monoxide sensor, *J. Phys. Chem. B* 103 (1999) 4412–4422.
- Y. Li, B. Xu, Y. Fan, N. Feng, A. Qiu, J. He, H. Yang, Y. Chen, The effect of titania polymorph on the strong metal-support interaction of Pd/TiO₂ catalysts and their application in the liquid phase selective hydrogenation of long chain alkadienes, *J. Mol. Catal. A Chem.* 216 (2004) 107–114.
- G. Bromiley, A. Shiryayev, Neutron irradiation and post-irradiation annealing of rutile (TiO_{2-x}): effect on hydrogen incorporation and optical absorption, *Phys. Chem. Miner.* 33 (2006) 426–434.
- F. Amano, M. Nakata, A. Yamamoto, T. Tanaka, Effect of Ti³⁺ ions and conduction band electrons on photocatalytic and photoelectrochemical activity of rutile titania for water oxidation, *J. Phys. Chem. C* 120 (2016) 6467–6474.

- [45] C. Kumar, N. Gopal, T. Wang, M. Wong, S. Ke, EPR investigation of TiO₂ nanoparticles with temperature-dependent properties, *J. Phys. Chem. B* 110 (2006) 5223–5229.
- [46] Y. Tamaki, K. Hara, R. Katoh, M. Tachiya, A. Furube, Femtosecond visible-to-IR spectroscopy of TiO₂ nanocrystalline films: elucidation of the electron mobility before deep trapping, *J. Phys. Chem. C* 113 (2009) 11741–11746.
- [47] J. Li, M. Zhang, Z. Guan, Q. Li, C. He, J. Yang, Synergistic effect of surface and bulk single-electron-trapped oxygen vacancy of TiO₂ in the photocatalytic reduction of CO₂, *Appl. Catal. B: Environ.* 206 (2017) 300–307.
- [48] D. Matthey, J. Wang, S. Wendt, J. Matthiesen, R. Schaub, E. Lægsgaard, B. Hammer, F. Besenbacher, Enhanced bonding of gold nanoparticles on oxidized TiO₂ (110), *Science* 315 (2007) 1692.
- [49] Z. Fang, B. Bart, E. Dirk, A. Roland, Defect-engineered metal-organic frameworks, *Angew. Chem. Int. Ed.* 54 (2015) 7234–7254.
- [50] X. Wang, Z. Rui, Y. Zeng, H. Ji, Z. Du, Q. Rao, Synergetic effect of oxygen vacancy and Pd site on the interaction between Pd/Anatase TiO₂(101) and formaldehyde: a density functional theory study, *Catal. Today* 297 (2017) 151–158.
- [51] S. Tauster, S. Fung, R. Garten, Strong metal-support interactions group 8 noble metals supported on TiO₂, *J. Am. Chem. Soc.* 100 (1978) 170–175.
- [52] M. Vannice, C. Twu, S. Moon, SMSI effects on CO adsorption and hydrogenation on Pt catalysts: I. Infrared spectra of adsorbed CO prior to and during reaction conditions, *J. Catal.* 79 (1983) 70–80.
- [53] E. Benvenutti, L. Franken, C. Moro, C. Davanzo, FTIR study of hydrogen and carbon monoxide adsorption on Pt/TiO₂, Pt/ZrO₂, and Pt/Al₂O₃, *Langmuir* 15 (1999) 8140–8146.
- [54] L. Liotta, G. Deganello, P. Delichere, C. Leclercq, G. Martin, Localization of alkali metal ions in sodium-promoted palladium catalysts as studied by low energy ion scattering and transmission electron microscopy, *J. Catal.* 164 (1996) 334–340.
- [55] X. Wang, X. Zou, Z. Rui, Y. Wang, H. Ji, Highly dispersed and active Pd nanoparticles over titania support through engineering oxygen vacancies and their anchoring effect, *Aiche J.* (2020) e16288n/a.
- [56] D. Wang, Y. Peng, S. Xiong, B. Li, L. Gan, C. Lu, J. Chen, Y. Ma, J. Li, De-reducibility mechanism of titanium on maghemite catalysts for the SCR reaction: an in situ DRIFTS and quantitative kinetics study, *Appl. Catal. B: Environ.* 221 (2018) 556–564.
- [57] H. Tan, J. Wang, S. Yu, K. Zhou, Support morphology-dependent catalytic activity of Pd/CeO₂ for formaldehyde oxidation, *Environ. Sci. Technol.* 49 (2015) 8675–8682.
- [58] C. Zhang, H. He, A comparative study of TiO₂ supported noble metal catalysts for the oxidation of formaldehyde at room temperature, *Catal. Today* 126 (2007) 345–350.
- [59] Z. Xu, J. Yu, M. Jaroniec, Efficient catalytic removal of formaldehyde at room temperature using AlOOH nanoflakes with deposited Pt, *Appl. Catal. B: Environ.* 163 (2015) 306–312.
- [60] T. Yang, Y. Huo, Y. Liu, Z. Rui, H. Ji, Efficient formaldehyde oxidation over nickel hydroxide promoted Pt/ γ -Al₂O₃ with a low Pt content, *Appl. Catal. B: Environ.* 200 (2017) 543–551.
- [61] L. Zeng, W. Song, M. Li, D. Zeng, C. Xie, Catalytic oxidation of formaldehyde on surface of HTiO₂/HCTiO₂ without light illumination at room temperature, *Appl. Catal. B: Environ.* 147 (2014) 490–498.
- [62] W. Cui, D. Xue, X. Yuan, B. Zheng, M. Jia, W. Zhang, Acid-treated TiO₂ nanobelt supported platinum nanoparticles for the catalytic oxidation of formaldehyde at ambient conditions, *Appl. Surf. Sci.* 411 (2017) 105–112.
- [63] L. Nie, J. Yu, M. Jaroniec, F. Tao, Room-temperature catalytic oxidation of formaldehyde on catalysts, *Catal. Sci. Technol.* 6 (2016) 3649–3669.
- [64] P. Tripodi, D. Gioacchino, J. Vinko, A review of high temperature superconducting property of pdh system, *Int. J. Mod. Phys. B* 21 (2007) 3343–3347.
- [65] H. Zhu, Z. Qin, W. Shan, W. Shen, J. Wang, Pd/CeO₂-TiO₂ catalyst for CO oxidation at low temperature: a TPR study with H₂ and CO as reducing agents, *J. Catal.* 225 (2004) 267–277.
- [66] C. Ma, C. Yang, B. Wang, C. Chen, F. Wang, X. Yao, M. Song, Effects of H₂O on HCHO and CO oxidation at room-temperature catalyzed by MCo₂O₄ (M = Mn, Ce and Cu) materials, *Appl. Catal. B: Environ.* 254 (2019) 76–85.
- [67] H. Chen, M. Tang, Z. Rui, X. Wang, H. Ji, ZnO modified TiO₂ nanotube array supported Pt catalyst for HCHO removal under mild conditions, *Catal. Today* 264 (2016) 23–30.
- [68] X. Yang, X. Yu, M. Lin, M. Ge, Y. Zhao, F. Wang, Interface effect of mixed phase Pt/ZrO₂ catalysts for HCHO oxidation at ambient temperature, *J. Mater. Chem. A* 5 (2017) 13799–13806.
- [69] M. Huang, Y. Li, M. Li, J. Zhao, Y. Zhu, C. Wang, V. Sharma, Active site-directed tandem catalysis on single platinum nanoparticles for efficient and stable oxidation of formaldehyde at room temperature, *Environ. Sci. Technol.* 53 (2019) 3610–3619.